Article

In Silico CFD Investigation of the Granulation Hydrodynamics in Rotating Drum: Process Sensitivity to the Operating Parameters and Drag Models

Safae Elmisaoui [1,2,*], Saad Benjelloun [1,*], Radouan Boukharfane [1], Lhachmi Khamar [2,3], Sanae Elmisaoui [1,2,4] and Mohamed Khamar [2]

1   MSDA Group, Mohammed VI Polytechnic University (UM6P), Ben Guerir 43150, Morocco
2   LGCE, Higher School of Technology in Salé, Mohammed V University in Rabat, Rabat 10100, Morocco
3   ENSA-Khouribga, Sultan Moulay Slimane University, LIPIM, Beni-Mellal 23000, Morocco
4   Laboratoire Réactions et Génie des Procédés, CNRS-ENSIC, Université de Lorraine, CEDEX, 54500 Nancy, France
*   Correspondence: safae.elmisaoui@um6p.ma (S.E.); saad.benjelloun@um6p.ma (S.B.)

Abstract: Computational fluid dynamics (CFD) have been extensively used to simulate the hydrodynamics of multiphase flows (MPFs) in rotating machinery. In the presence of a granular dense phase, the Kinetic Theory of Granular Flow (KTGF) is usually coupled to Eulerian multi-fluid models to obtain tractable computational fluid models. In the present work, the hydrodynamic behavior of a three dimensional, industrial scale, and rotating drum granulator with gas–solid flows is assessed using the Eulerian–Eulerian approach coupled with the k-ε standard turbulence model. A Eulerian–Eulerian Two-Fluid Model (TFM) is used with the KTGF model for the granular phase. The sensitivities to different operating parameters, including the rotational speed (8, 16, and 24 rpm), inclination degree (3.57°, 5.57°, and 7.57°), and degree of filling (20%, 30%, and 40%) are studied. Moreover, the impact of the drag model on the simulation accuracy is investigated. The flow behavior, regime transitions, and particle distribution are numerically evaluated, while varying the operating conditions and the drag models. The rotational speed and filling degree appear to have greater influences on the granulation effectiveness than on the inclination degree. Three drag models are retained in our analysis. Both the Gidaspow and Wen and Yu models successfully predict the two-phase flow in comparison to the Syamlal and O'Brien model, which seems to underestimate the hydrodynamics of the flow in both its axial and radial distributions (a fill level less than 35%). The methodology followed in the current work lays the first stone for the optimization of the phosphates fertilizer wet-granulation process within an industrial installation.

Keywords: granulation; Euler–Euler approach; process intensification; kinetic theory of granular flow; process optimization

1. Introduction

The main objective of the industrial processing of phosphate minerals is the production of granular fertilizers that are soluble and directly assimilable by plants. One of the unit operations in the manufacturing process of fertilizers is wet granulation [1]. The granulation essentially aims at forming agglomerates of a well-defined size that is generally larger than the initial particle size. The process also targets specific physico-chemical properties for the phosphate fertilizer grains: the particle size distribution, density, porosity, solidity, and residual water content [2].

The wet-granulation process is based on different technologies with different designs and mechanisms depending on the physico-chemical properties of the input product [3,4]. A wide range of granulation devices is found at the industrial scale, including fluidized bed

granulators [5], high shear mixer granulators [6], rotating drum granulators [7], and pan granulators [8] (cf. Figure 1).
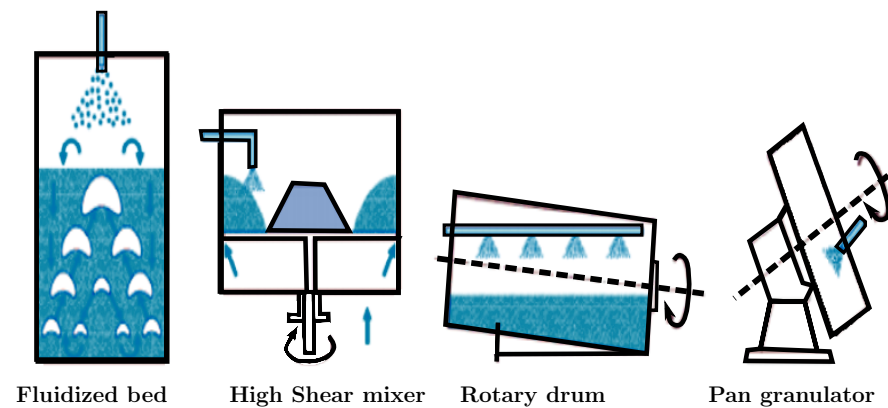

Figure 1. Wet-granulation technologies. Inspired from Saleh and Guigon [3].

Due to their economical aspects and their easy manipulation, rotating drums are widely used for the wet granulation of fertilizer particles. In this process, a slurry that results from (i) the neutralization of dilute phosphoric acid solution with ammonia [9] and (ii) the crystallization of the product is injected into a rotating drum granulator [10]. This process has the added advantage of including drying, which reduces the humidity ratio [7,8], and coating, which improves the effectiveness of the products depending on the soil characteristics [11].

Despite the wide employment of rotating drums in the phosphate fertilizer industry, these are still challenging equipment that require a complex adaptation of the operating conditions to the quality of the raw material feeding the process [12]. Depending on the operating parameters, the physical properties of materials, and the geometrical designs, rotating drums can show different flow regimes for the particle dynamics [13]. The flow regime significantly affects the quality of material processing in terms of mixing, grinding, size enlargement, etc. Experimental studies conducted by Arntz et al. [14] showed that rotating drums can exhibit seven flow regimes: Sliding, surging, slumping, rolling, cascading, cataracting and centrifuging [15]. Each regime is characterized by its specific hydrodynamics [16].

Currently, the increase in computing capabilities makes numerical simulation affordable to study the particle dynamics in rotating drums. Several studies have proven the Computational Fluid Dynamics (CFD) efficiency for granular flow assessment and analysis. For these simulations, the Euler–Euler approach [17], Euler–Lagrange approach, Discrete Element Method (DEM) [18,19] and Population Balance Model (PBM) are frequently used methods for dense granular flow studies.

Coupled CFD-DEM [20], CFD-PBM, DEM-PBM [21,22], and CFD-DEM-PBM models were developed for better prediction and understanding of the hydrodynamics and phase interactions [23]. The Euler–Euler approach considers the fluid and solid phases as interpenetrating continua, coupled through interaction terms. The solid phase properties are obtained using the kinetic theory of granular flow.

The relative computational efficiency of this approach with respect to the other ones cited above, as well as the fast development in computational resources allow it to replace, at least partially, experimental studies while providing a way to analyze phenomena that are hardly studied experimentally. Yet, great attention should be given to the interaction models. In particular, the interphase momentum exchange models are key components for accurate multiphase CFD simulation. Several research works [24] have shown that the drag model is the critical closure model to accurately predict the hydrodynamics in multiphase gas–solid flows.

However, none of these studies analyzed the flow behavior in a large scale, rotating and three-dimensional model, such as a granulation drum. Moreover, the range of validity for each model should be assessed. Accurate numerical prediction of the hydrodynamics can then be used for optimization of the process key operating parameters on the light of the regime transition theory [14,15].

In the present work, a CFD simulation of the multiphase flow within an industrial rotating drum granulator is performed. The aim of this study is twofold: to analyze the sensitivity of the rotating drum granulator to three operating parameters—namely, the rotational speed, fill level and the inclination degree; and to evaluate their effects on the hydrodynamics. The gas–solid two-fluid flow inside the inclined rotating drum granulator is considered, and the Eulerian–Eulerian mathematical model describing the multi-phase flow is presented in Section 2.

The three evaluated drag models (Gidaspow; Syamlal and O'Brien; and Wen and Yu) are also presented. After presenting the physical and numerical parameters for the simulation setting in Section 3, the flow predictions are discussed in Section 4, focusing on the radial and axial particle distribution dependence to the granulator rotational speed (8, 16, and 24 rpm), fill level (20%, 30%, 40%) and the inclination degree (3.57°, 5.57°, and 7.57°). The accuracy of the hydrodynamics prediction is analyzed, and the validity range of some effective parameters is proposed for the different operating conditions.

2. CFD Model Setup

As mentioned above, the Eulerian–Eulerian unsteady TFM is used in its general formalism. The governing equations of fluid mechanics are solved by the CFD software ANSYS Fluent 2020 R1 solver (CADFEM, AN2, Ben Guerir, Morocco) . In the framework of TFM, both the gas phase and the solid phase are solved as continuous fluids interspersed with each other. The dynamic characteristics of the solid phase are assumed to be the same as those of the gas phase, and thus it can be described with the equation of conservation of fluid mechanics. The solids stress terms are closed by the kinetic theory of granular flow [25], and the interaction between the gas and solid phase is coupled through drag force.

2.1. Governing Equations and Fluid-Solid Interactions

Neglecting the effect of compressibility, the continuity equations for gas–solid mass conservation are represented by the following equations:

$$
\begin{aligned}
\nabla \cdot \left(\alpha_g \mathbf{v}_g \varrho_g \right) &= 0, \\
\nabla \cdot \left(\alpha_s \mathbf{v}_s \varrho_s \right) &= 0,
\end{aligned}
\tag{1}
$$

where the subscripts g and s stand for the gas phase (air) and the solid phase (particles), respectively. In Equation (1), α, ϱ, and $\mathbf{v}$ stand for the volume fraction, density, and velocity, respectively, with $\alpha_g + \alpha_s = 1$. The conservation of the gas and solid momentum is given by the following equations

$$
\begin{aligned}
&\frac{\partial}{\partial t} \left(\alpha_g \varrho_g \mathbf{v}_g \right) + \nabla \cdot \left(\alpha_g \varrho_g \mathbf{v}_g \mathbf{v}_g \right) = -\alpha_g \nabla p + \\
&\nabla \cdot \boldsymbol{\tau}_g + \alpha_g \varrho_g \mathbf{g} + \alpha_g \varrho_g \left(\mathbf{F}_g^{\text{ext}} + \mathbf{F}_g^{\text{lift}} + \mathbf{F}_g^{\text{vm}} \right) + \mathcal{K}_{gs} \left(\mathbf{v}_s - \mathbf{v_g} \right),
\end{aligned}
\tag{2}
$$

$$
\begin{aligned}
&\frac{\partial}{\partial t} \left(\alpha_s \varrho_s \mathbf{v}_s \right) + \nabla \cdot \left(\alpha_s \varrho_s \mathbf{v}_s \mathbf{v}_s \right) = -\alpha_s \nabla p + \nabla p_s + \\
&\nabla \cdot \boldsymbol{\tau}_s + \alpha_s \varrho_s \mathbf{g} + \alpha_s \varrho_s \left(\mathbf{F}_s^{\text{ext}} + \mathbf{F}_s^{\text{lift}} + \mathbf{F}_s^{\text{vm}} \right) + \mathcal{K}_{gs} \left(\mathbf{v}_g - \mathbf{v}_s \right),
\end{aligned}
\tag{3}
$$

where $\mathbf{F}_q^{\text{ext}}$ (q stand either for g or s), $\mathbf{F}_q^{\text{lift}}$, and $\mathbf{F}_q^{\text{vm}}$ are the external body force, the lift force, and the virtual mass force, respectively. $\boldsymbol{\tau}_q$ are the phase stress tensors given by:

$$
\begin{aligned}
\boldsymbol{\tau}_g &= \alpha_g \mu_g \left(\nabla \mathbf{v}_g + \nabla \mathbf{v}_g^{\mathsf{T}} \right) \\
\boldsymbol{\tau}_s &= \alpha_s \mu_s \left(\nabla \mathbf{v}_s + \nabla \mathbf{v}_s^{\mathsf{T}} \right) + \alpha_s \left(\lambda_s - \tfrac{2}{3} \mu_s \right) \nabla \cdot \mathbf{v}_s \mathbb{I}
\end{aligned}
\tag{4}
$$

$\mathcal{K}_{sg}$ is the momentum drag exchange coefficient between the phases. In the current investigation, we assume that the system is isothermal, and only drag and gravity forces are considered. Indeed, many research studies [18,24] concluded that the effects of the lift and virtual mass forces are negligible compared to the drag force impact.

We confirmed this with three simulation cases. The momentum exchange coefficient $\mathcal{K}_{sg}$ between the solid phase s and fluid phase g can be written in the following general form

$$\mathcal{K}_{sg} = \frac{\alpha_s \varrho_s f_d}{\varpi_s},$$

where f_d is the drag function and ϖ_s is the particulate relaxation time defined as

$$\varpi_s = \frac{\varrho_s d_s^2}{18 \mu_g},$$

where d_s is the diameter of particles in the solid phase and μ_g is the air viscosity. The definition of the drag function f_d includes a drag coefficient $\mathcal{C}_d$ that is based on the relative Reynolds number $\mathcal{R}e_r$ defined as

$$\mathcal{R}e_r = \frac{\varrho_f |\mathbf{v}_g - \mathbf{v}_b| d_s}{\mu_g}. \tag{5}$$

For the $\mathcal{C}_d$ coefficient, different empirical and semi-empirical models exist, and some will be presented in the next subsection.

2.2. Drag Forces

The principal closure model for the momentum exchange equation is the drag force. The literature reports numerous drag models employed in CFD simulations of multiphase systems containing a granular phase. Here, we aim to investigate the influence of the drag model on the computation of the granular flow in a rotating drum granulator. Several research works on drag models in fluid–solid systems give a recommendation of drag models depending on the density of the granular phase [26–28].

The Schiller and Naumann [29] and Helland et al. [30] models are recommended for thin and diluted systems. However, for multiphase systems with a dense granular phase, three models are preferred and are retained for further investigation in the present study. The first one was developed by Wen and Yu [31] and is given by

$$\mathcal{K}_{sg} = \frac{3\mathcal{C}_d \alpha_s \alpha_g \varrho_g |\mathbf{v}_s - \mathbf{v}_g|}{4 d_s} \alpha_g^{-2.65} \tag{6}$$

where

$$\mathcal{C}_d = \frac{24}{\alpha_g \mathcal{R}e_s} \left[1 + 0.15 (\alpha_g \mathcal{R}e_s)^{0.687} \right]. \tag{7}$$

The second one was introduced by Gidaspow [32] to correct Wen and Yu [31]'s model following the expression

$$\mathcal{K}_{sg} = \begin{cases} \frac{3\mathcal{C}_d \alpha_s \alpha_g \varrho_g |\mathbf{v}_s - \mathbf{v}_g|}{4 d_s} \alpha_g^{-2.65} & \text{for} \quad \alpha_g > 0.8, \\ \frac{150 \alpha_s (1 - \alpha_g) \mu_g}{\alpha_g d_s^2} + \frac{1.75 \varrho_g \alpha_s}{d_s} |\mathbf{v}_s - \mathbf{v}_g| & \text{for} \quad \alpha_g \leqslant 0.8. \end{cases} \tag{8}$$

The third considered model is due to Syamlal and O'Brien [33], and it can be expressed as:

$$\mathcal{K}_{sg} = \frac{3\mathcal{C}_d \alpha_s \alpha_g \varrho_g}{4 V_{r,s}^2 d_s} \left(\frac{\mathcal{R}e_s}{V_{r,s}} \right) |\mathbf{v}_s - \mathbf{v}_g|, \tag{9}$$

where

$$\mathcal{C}_d = \left(0.63 + \frac{4.8\sqrt{V_{rs}}}{\sqrt{Re_s}}\right)^2, \tag{10}$$

with

$$V_{r,s} = 0.5\left(A - 0.06\mathcal{R}e_s + \sqrt{(0.06\mathcal{R}e_s)^2 + 0.12\mathcal{R}e_s(2B - A) + A^2}\right), \tag{11}$$

and

$$A = \alpha_g^{4.14}, \quad B = \begin{cases} 0.8\alpha_g^{1.28} & \text{for } \alpha_g \leq 0.85 \\ \alpha_g^{2.65} & \text{for } \alpha_g > 0.85 \end{cases} \tag{12}$$

2.3. Solid-Solid Interactions

To model the particle–particle interactions, the KTGF is used to define the stress term τ [34]. This theory is based on an analogy with the classical kinetic gas theory. For instance, a term θ_s, representing the granular temperature, also called "pseudo-thermal", accounts for the kinetic energy associated with the particle velocity fluctuations [35].

The transport equation for the granular temperature is expressed as follows,

$$\frac{3}{2}\left[\frac{\partial}{\partial t}(\varrho_s\alpha_s\theta_s) + \nabla\cdot(\varrho_s\alpha_s\mathbf{v}_s\theta_s)\right] = (-p_s\mathbb{I} + \boldsymbol{\tau}_s) : \nabla\mathbf{v}_s + \\ \nabla\cdot(k_{\theta_s}\nabla\theta_s) - \gamma_{\theta_s} - 3\mathcal{K}_{sg}\Phi_{gs}, \tag{13}$$

where $(-p_sI + \boldsymbol{\tau}_s) : \nabla\mathbf{v}_s$ represents the resultant energy from the solid stress tensor, $\nabla\cdot(k_{\theta_s}\nabla\theta_s)$ is the diffusion of energy, Φ_{gs} is the energy exchange between the fluid and solid phases, k_{θ_s} is the diffusion coefficient, and γ_{θ_s} is the collisional dissipation energy given by [36]:

$$\gamma_{\theta_s} = \frac{12(1 - e_{ss}^2)\alpha_s^2\varrho_sg_0\theta_s^{3/2}}{d_s\sqrt{\pi}}, \tag{14}$$

and

$$\theta_s = \frac{1}{3}u_{s,i}^2, \tag{15}$$

where e_{ss} is the restitution coefficient for particle collisions, taken as 0.95, and the radial distribution function g_0 represents the probability of interparticle contact. Neglecting the convective and diffusive terms in Equation (13) allows reducing the transport equation for the granular temperature to the algebraic form

$$(-p_sI + \boldsymbol{\tau}_s) : \nabla\mathbf{v}_s - \gamma_{\theta_s} - 3\mathcal{K}_{sg}\Phi_{gs} = 0. \tag{16}$$

To estimate the viscosity of the solid phase μ_s, three terms are used:

$$\mu_s = \mu_s^{\text{fr}} + \mu_s^{\text{col}} + \mu_s^{\text{kin}}, \tag{17}$$

where μ_s^{fr} is the frictional viscosity, μ_s^{col} is the collisional viscosity, and μ_s^{kin} is the kinetic viscosity, which are modeled using detailed correlations that can be found in Schaeffer [37].

3. Numerical Model Setup

The numerical simulations are performed for a three dimensional domain with the real industrial scale dimensions. The rotating drum granulator geometry and generated mesh were developed using ANSYS Design Modeler and ANSYS mesher, respectively. The granulator consists of a cylindrical inclined drum of diameter $D = 4.5$ m and length $L = 9.0$ m. The cylinder is inclined from the lateral plane with 3.57° in the nominal industrial conditions.

To perform the grid independence analysis, we created three meshes with different grid refinement qualities. The meshing used tetrahedral hybrid meshes with a grid of up to 2×10^5 cells. The influence of mesh size on the rotating drum simulations is pre-

sented in Section 3.2. The second order upwind scheme was adopted to discretize the governing equations, while the QUICK scheme was employed for the volume fraction transport equation.

For the pressure–velocity coupling algorithm, the pressure-based coupled SIMPLE algorithm was adopted. The transient CFD calculations were performed, with the time step size of 10^{-4} s and maximum of 20 iterations per time step. We defined 10^{-4} as a time step value to allow the rotary drum to rotate for more seven complete rotational cycles and to ensure convergence for all the rotational speeds and operating points without then need to tune this parameter for each simulation. In order to match a local stability criteria based on the Courant number (CFL) to achieve temporal accuracy and numerical stability, the maximum allowed value of Courant number was 0.7. For all system equations, the residual was set to 10^{-3}.

3.1. Physical Parameters

The primary phase is defined by air, and the secondary phase is formed by the solid fertilizer particles. The particle size distribution effect was neglected, and the averaged particles diameter was set to 2 mm. The physical characteristics of the particles and air are summarized in Table 1.

Table 1. Physical properties of the simulations.

Physical Property	Value
Air density (ϱ_g)	1.255 kg/m^3
Air viscosity (μ_g)	1.7894×10^{-5} kg/m·s
Fertilizer particles density (ϱ_s)	1574 kg/m^3
Fertilizer particles diameter (d_s)	2 mm

The drum is initially filled with a fertilizer particle bed and is operated in batch mode. The wall of the drum is rotating with a rotational speed set for each simulation. It is assumed to be a non-slip wall that conveys the necessary shear traction to the granular flow as shown by Figure 2. Generally, the products feed the granulator from the upper zone (inlet) and leave from the lower zone (Outlet). In this simulation, the batch mode is ensured by the definition of these boundaries as rebound periodic conditions.

(a) (b)
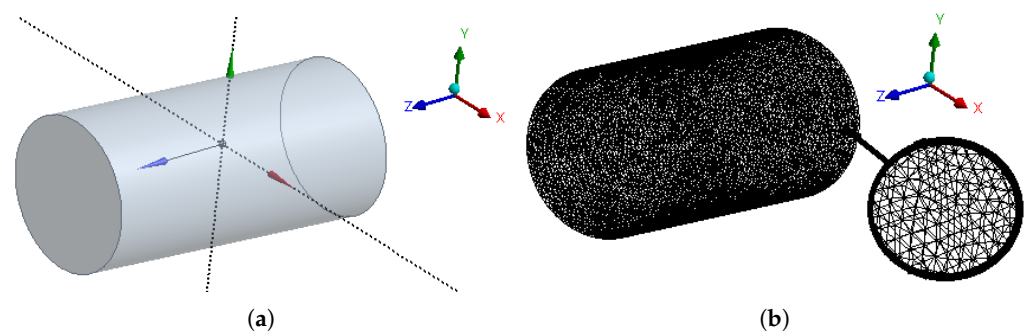
**Figure 2.** CAD and mesh of the simulation domain. (**a**) CAD Geometry. (**b**) Mesh of the geometry.

To investigate the fertilizer particle dynamics using the Eulerian approach, different drag models were evaluated using different operating conditions. Three different values of rotational speeds, filling degrees, and inclination degrees, for the three different drag models, were evaluated as shown in Table 2. Hence, the total number of simulation cases was 81. The average CPU time was 576 core-hours per transient simulation of physical time 200 s.

Table 2. Details of the CFD simulated scenarios.

Parameter	Tested Options		
Rotational speed (rpm)	8	16	24
Inclination degree (°)	3.5	5.5	7.5
Filling degree (%)	20	30	40
Drag model	Gidaspow [32]	Syamlal and O'Brien [33]	Wen and Yu [31]

3.2. Mesh Independence Analysis

The assessment of mesh convergence was performed with three levels of mesh refinement as shown in Figure 3.
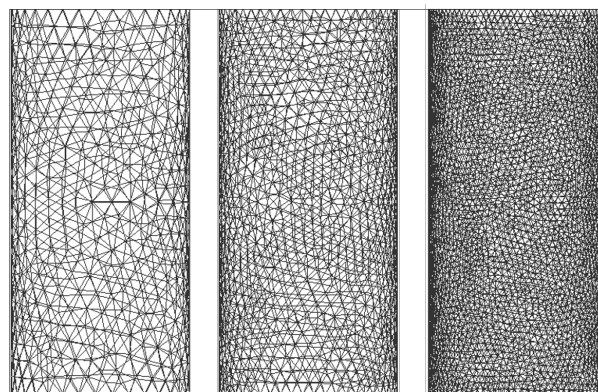
Figure 3. Meshes for the mesh convergence study.

The computational domain was discretized using the three meshes containing 20,700 (coarse), 170,625 (medium), and 266,045 (fine) quadrilateral cells. The two-phase simulation tfg considered for the grid independence/convergence analysis. For the wall layer modeling and for the three mesh grid qualities, we ensured y^+ in the range of 10–300 [38]. The y^+ prediction also takes into consideration the rotating walls. An averaged value of $y^+ < 100$ in all internal domains, and $y^+ < 11$ for near the wall cells were respected in the meshing procedure.

For the initial instant ($t = 0$ s), the radial distribution of the two-phases can be observed in Figure 4. The mesh refinement impact on capturing the interphase surface is clear.
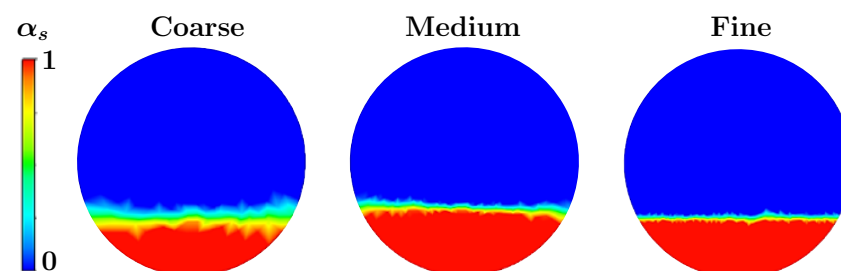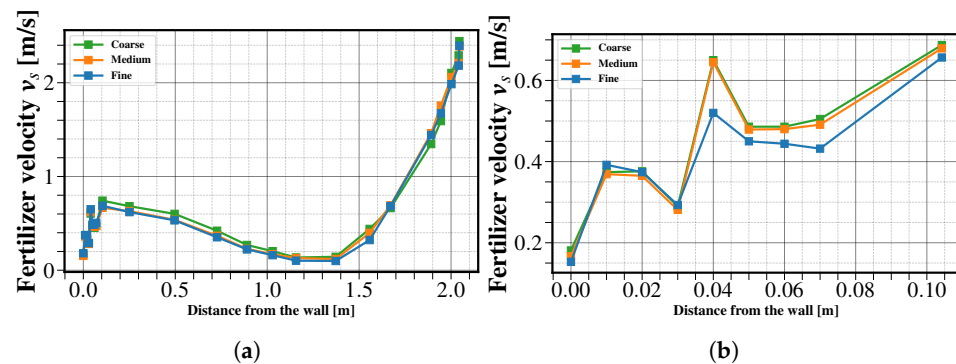

Figure 4. Radial cross section at the initial time for the different meshes.

Figure 5 presents the velocity magnitude over the perpendicular line to the particle bed in the simulation domain (x–y plane, $y = 2.5$ m, and $z = 4$ m).

Figure 5. The velocity magnitude of particles (m/s) as a function of the distance (**a**) from the wall and (**b**) zoom in close to the wall for the case (8 rpm, 30% filling degree, and 3.57° inclination degree).

Following these results, the difference between numerical predictions obtained using the refined and the medium grids is negligible, and the medium grid featuring 170,625 cells is retained to maintain reasonable computational costs.

4. Results and Discussion

Mass, heat, and momentum transfer efficiency within rotary drums depends on the flow hydrodynamics. Thereby, the understanding of the flow regimes is fundamental to determine the undesirable conditions to avoid when monitoring this unit operation. For rotating drum models with a dense solid phase, the lift, virtual mass, and wall friction parameters can be negligible compared to the gravity and drag model impacts on the solid phase flow prediction [39].

We confirmed this for the present computational model with three simulation cases. However, the global CFD model is sensitive to the drag model [24,40,41]. In the following, an analysis of the flow hydrodynamics and the sensitivity to the drag models, rotational speed, and filling level is performed to deepen our understanding of the dynamic behavior of granular flow in rotating drums.

4.1. Drag Model Effect on Hydrodynamics Predictions

4.1.1. Effect on the Particle Velocity

The time-averaged results obtained on the line located at a radial cross section in (x–y plane with $y = 2$ m and $z = 4.5$ m) of the drum are shown in Figure 6. The operating conditions were 30% of the fill rate (which is equivalent to 0.675 m as the granular bed depth), 3.57° inclination degree from the reference plan, and a rotational speed of 8 rpm. For the three drag models, the fertilizer particle velocity profile had its highest value of 2.4 m/s at the bed surface and then decreased with the decreasing radial position to reach its lowest value at the active–passive zone interface, and then a reverse of the flow took place as a result of the drum wall.

The lowest particle velocity on the profile depends slightly on the drag model, and Syamlal and O'Brien [33]'s correlation appears to overestimate it in comparison with the other two drag models. Note that the used conditions ensure a rolling regime, which generates a tumbling motion of solids within the rotary drum. The active region occupies a large part ensuring a maximum exchange of intra-particles in the upper zone of the bed.
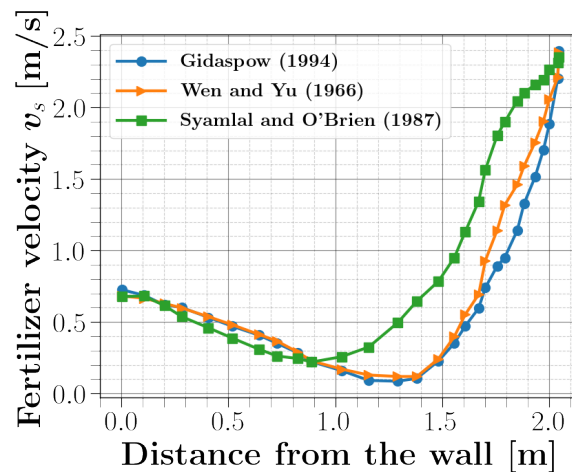
Figure 6. The fertilizer particle velocity distributions predicted using the three drag models for a rotational speed of 8 rpm and a 30% filling degree.

The predictive capabilities of CFD models in rotating drums has been assessed in many experiments. Santos et al. [42] showed that the employed drag models do not impact the CFD model prediction and, therefore, can be neglected. Other studies [28,43] highlight the crucial role of the drag model in the flow hydrodynamics prediction. In our study, the comparison results revealed that the particle velocity predictions were more accurate with the Gidaspow [32] and Wen and Yu [31] models than the predictions of the Syamlal and O'Brien [33] model. However, almost identical results were obtained using the Gidaspow [32] and Wen and Yu [31] models. As other CFD modeling studies have highlighted [44], we conclude that the Syamlal and O'Brien [33] drag model is not suitable for large scale flows.

4.1.2. Effect on the Two-Phase Volume Fraction Distribution

As the drag model is a dominant element in the particle interaction prediction with the priority to be defined in the CFD model over other CFD subcomponents (coalescence, breakage...) and to be combined with segregation model for robust further CFD simulations allowing for better particle hydrodynamics predictions. In this section, we aim to validate our observations on drag models effects and their ability to accurately predict the particle phase. A projection of the drum on a transversal middle plane is considered to quantify the axial dispersion of fertilizer particles at different simulation times (see Figure 7).

At the beginning of the drum rotation ($t = 5$ s), the interface between air and a solid bed conserves its initial flat pattern. Afterwards, at $t = 10$ s, a portion of the particles reaches the top of the drum, and a fraction of particles adheres to the wall of the drum. On the other hand, due to the drum's inclination, most particles are stacked in the lower zone and do not reach the top of the drum. The gravitational forces acting on particles in the axial direction dominate the velocity axial component, and most particles accumulate near the bottom of the drum. At $t = 20$ s, most particles from the active zone attain the higher part of the drum and an S-shape surface appears on the cross section plane with significant curvature announcing a transition from the rolling to the cascading regime.

Considering the effect of rotation, the bed is more expanded, which increases the action of inertial forces on the fertilizer grains. However, granular layers with lower density and higher surface velocity favor regime transition. From Figure 7, the effect of the drag model on the evolution of the solid bed distribution is not significant. It is worth noting that an important phenomenon occurs at this stage: the upper percentage of fertilizer particles that reaches the top of the drum cannot resist a flow continuity indicating an avalanche wave, and particles return to the granular bed, which directly impacts the mixing

quality within the drum and, furthermore, favor inter-particle interactions for coalescence, breakage, and other mechanisms.
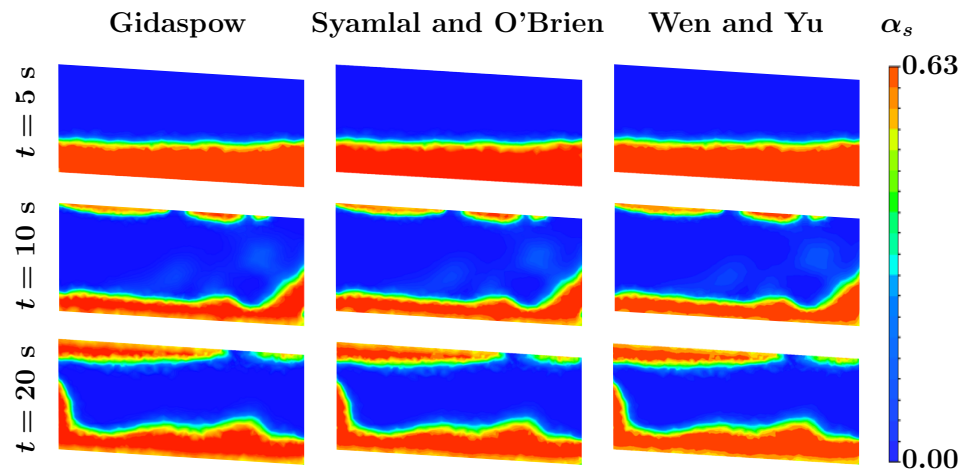

Figure 7. Front view of a middle transversal plane of particle axial distribution with different drag models at different simulation times with a 30% fill rate α_s (particle volume fraction), a domain rotational speed of 8 rpm, and an inclination of 3.57°.

4.2. Flow Sensitivity to Operating Conditions

4.2.1. Rotational Speed Effect

In this section, the effects of rotational speeds on particle dynamics are investigated. Rotational speed is a key parameter for controlling the particle dynamics inside the granulator. The variations of the particles' average velocity at the x–y middle plane with $y = 2.25$ m in the drum are portrayed in Figure 8, for each drag model, for three rotational speeds of 8, 16, and 24 rpm, and for three filling levels of 20%, 30%, and 40%.
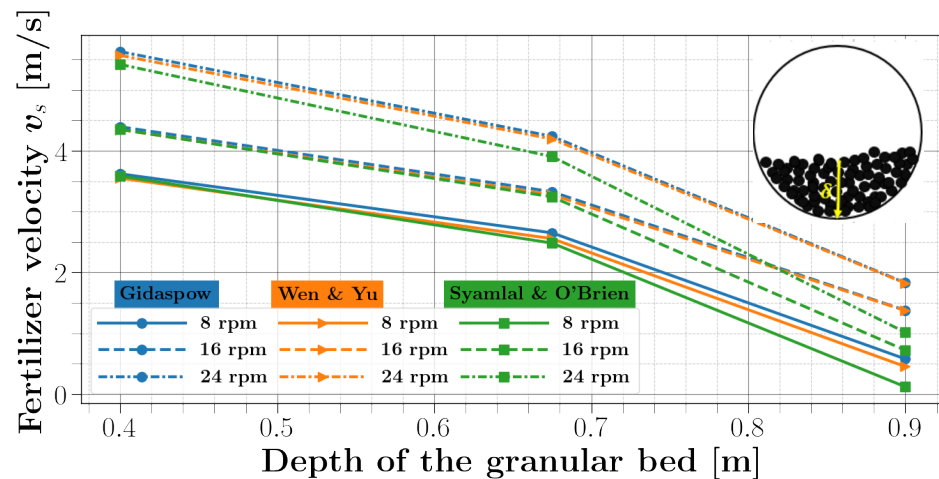
Figure 8. Particle velocity profile ($d = 2$ mm) for 8, 16, and 24 rpm rotational speeds with different drag models tested, with a representative snapshot of the depth of the granular bed δ (distance from the drum bottom to the interface between the granules and air).

The particle's velocity decreases with increasing bed depth. On the other hand, it considerably increases when increasing the rotational speed of the rotating drum. This is due to the transfer of the energy from the drum to the granular bed. The overall particle distribution within the granular bed can be explained by the fact that the thickness of the active layer is more considerable when the rotational speed is higher and the bed depth is lower; thus the fertilizer particles attain the highest mean velocity with a δ of 0.4 m (filling rate of 20%) and a maximal rotational speed of 24 rpm. Simultaneously increasing the

rotational speed and the depth of the granular bed leads to a decrease in the velocity of fertilizer particles.

This is due to a higher thickness of the passive layer in the granular bed, which reduces the fraction of particles in the active layer and slows the particle movement within the drum. The present findings agree well with the study performed by Wu et al. [45]. Moreover, at the different rotational speeds and fill levels, the predictions given by Gidaspow [32] and Wen and Yu [31] models are similar. Syamlal and O'Brien [33]'s model gives a prediction with a similar trend at low bed depths but deviates when increasing the bed depth.

We can conclude from these and Section 4.1 that, although we validated the observations from previous works [28] that recommended this drag model in non dense gas–solid systems, such as fluidized beds, we must note the limitations of this models for dense solid systems, such as rotating drums. The Gidaspow [32] and Wen and Yu [31] drag models are more accurate for gas–solid (dense) flows in rotating drums.

The granular temperature represents a key parameter in the KTGF model, since it allows measuring the degree of random particle motion (granular fluctuations due to the continuous intra-particle and particle–boundary collisions). Therefore, it could be used as a good indicator of the granular flow hydrodynamics in the rotating drum [46]. The contours of the granular temperature, θ_s, of fertilizer particles is displayed in Figure 9. The rotational speed seems to play an important role in the granular temperature. Indeed, increasing the rotation speed leads to an increase in the repose angle and a decrease in the mean circulation time of the particle, which improves the particles mixing in the bed.
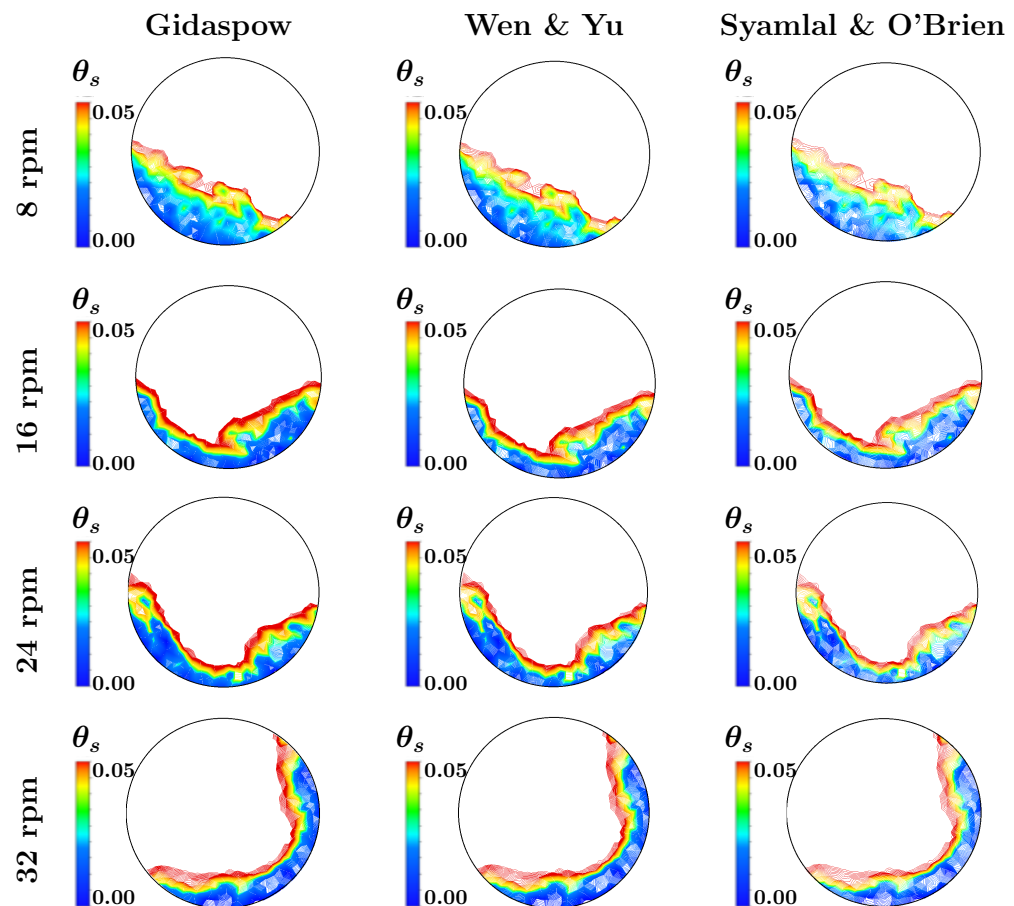

Figure 9. Axial snapshots of the granular temperature Θ_s ($m^2 \cdot s^{-2}$) patterns in drums rotating at 8, 16, 24, and 32 rpm with the three studied drag models at the end time of 200 s.

The particles in the passive layer turn in the upwards direction in a nearly solid body rotating fashion independently of the considered drag model. Note that the surface of the granular bed flattened as the rotation speed decreased. The heat appeared to be

transferred from the wall to the center of the bed, and the temperature showed concentric gradients for higher rotation speeds. This is compatible with previous experimental [47] and numerical [48] studies. The three drag models retained in this study give similar granular temperature flow patterns.

4.2.2. Filling Degree Effect

The rotating granulator was set to different rotational speeds in order to analyze the different regimes of solid motion. The results in Figure 10 show the transition between the typical transverse bed motions (rolling, cascading, and cataracting) during the rotation of the rotating drum. The configurations in Figure 10 represent the hydrodynamics in a radial section in the middle of the rotary granulator for three filling rates: 20%, 30%, and 40% of the solid granular phase. We present the results for a rotational speed of 8 rpm, which is the nominal speed in the industrial process. The Gidaspow [32] drag model is retained.
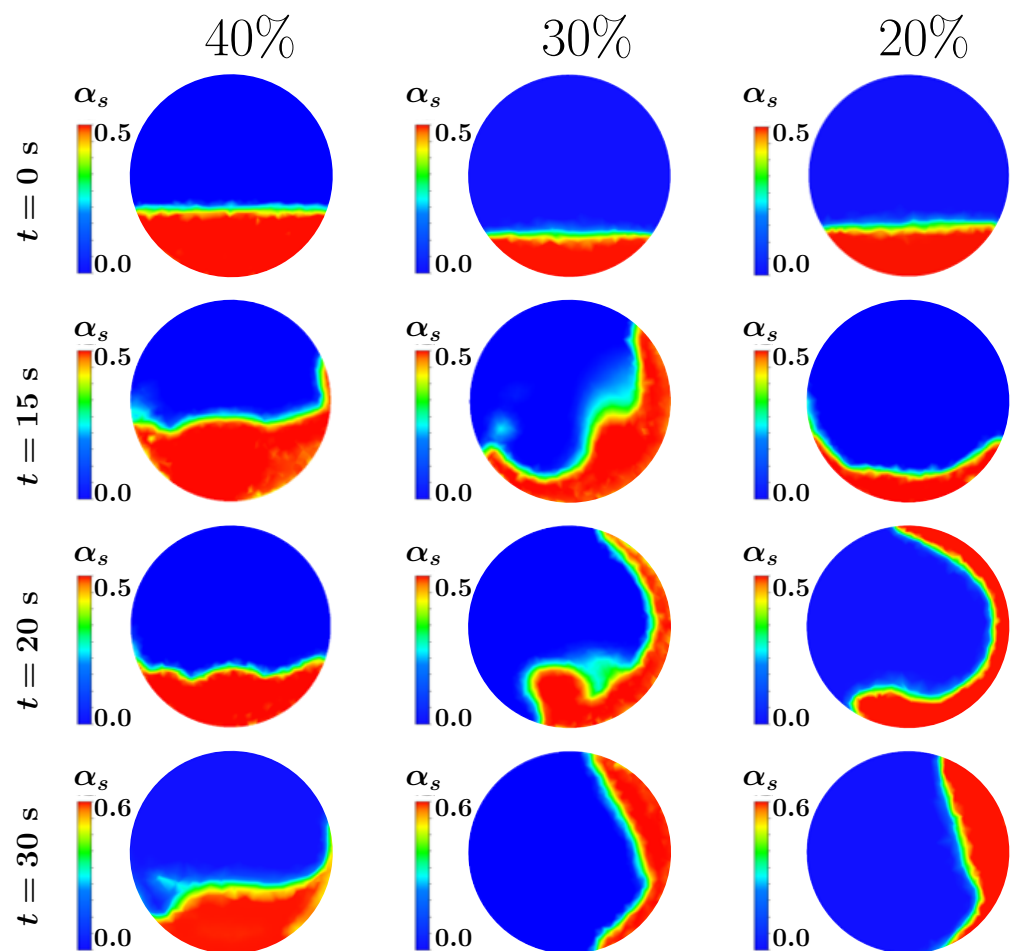
Figure 10. Volume fraction of the the granular solid phase for fill levels of 20%, 30%, and 40% for a drum rotating at 8 rpm.

The surface of the granular bed features important deformations in its active layer for filling rates of 20 and 30% but less deformations for the level of 40%. In this latter case, the bed keeps a sliding flow regime during the simulation, therefore, hindering good mixing in the granular bed and inhibiting the exchanges of mass, heat, and momentum between the granules. The case of a 20% and 30% filling rate allows the granular phase to easily follow the rotational movement of the granulator, and the active layer is thicker.

Indeed, a total adhesion to the walls of the domain was observed around the wall of the granulator until reaching the height threshold causing the avalanche phenomenon, and the granular bed was placed back at the bottom of the domain by gravity effect. This

effect was less accentuated when using a value of solid volume fraction of 20%, where the resistance to gravity was clearer, and the granular bed was more compact, whereas the critical flow regime of cataracting was reached. This is likely due to the fact that stronger frictional forces are formed between the particles, which leads to an increase in the cohesive force that can cause a transition from the rolling regime to the cataracting regime or to the centrifuging regime with higher rotational speeds. This is not favorable in the case of a reactive flow, for which certain exchange constraints between the phases must be respected.

The present results define a range of variation of filling rate to be respected with a minimum of 20% and a rate not to be reached of 40%. We note that, following the present results, the rolling regime is the most adequate to achieve good hydrodynamics within the granulator.

4.2.3. Inclination Degree Effect

The tailored numerical model was employed to investigate the effects of the inclination degree on the flow hydrodynamics along the rotating drum. Figure 11 represents the fertilizer particles averaged axial velocity along the rotating drum for different operating conditions, with a constant fill rate of 30%. It is clear that the particle axial velocity increases gradually along the drum. As a result, the axial component of the particle velocity is increasingly important by mass conservation.
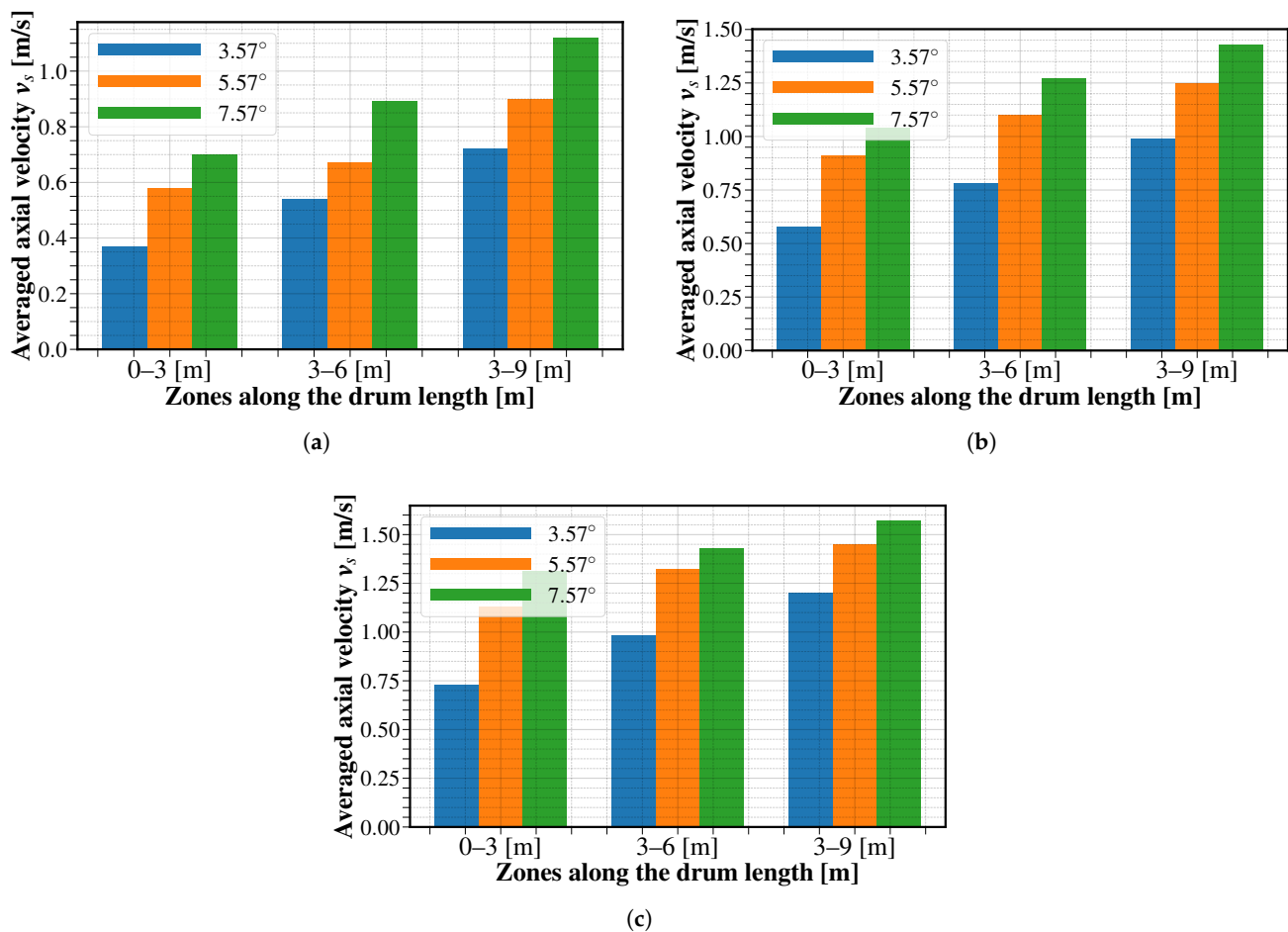
Figure 11. The axial particle velocity (m/s) distributions in three subdivision zones per drum length (m) for 8, 16, and 24 rpm rotational speeds. (**a**) 8 rpm. (**b**) 16 rpm. (**c**) 24 rpm.

On the other hand, the effect of the inclination degree on particle dynamics is varying along the drum length. By increasing the inclination slope, particles tend to occupy the lower end of the drum, due to the gravitational force component in the axial direction.

Figure 11 further displays that any increase in the inclination degree impacts the axial and radial particle distribution along the drum, which will enhance the mass and heat transfer mechanisms between the particles present in the active layer at the end part of the drum. The rest of the particles defining the passive region can present a dead granular bed depending on the fill rate.

Conjugated effects between the inclination degree and rotational speed are clearly observed in Figure 11. By increasing the rotational speed and the drum inclination, the particle volume fraction decreases in the inlet zone. Moreover, as the rotational speed increases, the effect of inclination decreases on the averaged velocity as expected. The impact of inclination on the mean axial velocity variation along the drum is less significant with the increase in rotational speed.

The variation in the axial velocity of particles along the rotating drum explains the regime transition phenomena previously mentioned, particularly for the rolling-cascading regimes by increasing the rotational speed with a 30% fill level. Similar observations were highlighted by the experimental study of Li et al. [49] and proven in experimental and simulation studies by Rogers et al. [50].

5. Conclusions

This paper investigated the impact of drag models on gas–solid simulation predictions and the influence of the operating conditions on fertilizer particle dynamics behavior. A two-phase three-dimensional CFD model of particle and fluid flows in rotary drums was developed using ANSYS Fluent. The model is provided for research reproducibility. The results of the present study proved that the drag model is a subcomponent that should have special attention in CFD model development.

A considerable influence on the predictions of the granular bed behavior was observed when testing the different drag models. Indeed, better predictions were obtained using Wen and Yu and Gidaspow drag models in the different studied cases covering the parameters range: rotational speed (8 rpm–32 rpm), filling level (20%–40%), and inclination degree (3.57°–7.57°). The Syamlal and O'Brien drag model gives accurate predictions for limited scenarios and, in particular, when the solid fraction is moderate (fill level $\preceq$ 35%).

Therefore, the Syamlal and O'Brien model is only suitable for rotating drums operating with a lower solid fraction. The CFD model was applied to study the effects of drum rotational speed, filling degree, and inclination degree on the multiphase flow and particle dynamics. The results confirmed the CFD model's ability to assess multiphase flow for industrial scale rotary drum systems.

In light of the present work, new operating conditions combinations are proposed for the industrial plant (for example: 16 rpm, 30%, 3.57°). An experimental campaign is planned on the industrial plant to further evaluate and compare the new candidate operating points.

Author Contributions: Conceptualization: S.E. (Safae Elmisaoui), L.K. and R.B.; methodology: S.E. (Safae Elmisaoui), L.K., S.E. (Sanae Elmisaoui) and R.B.; software: S.E. (Safae Elmisaoui); validation: S.E. (Safae Elmisaoui), L.K. and S.B.; formal analysis: S.E. (Safae Elmisaoui) and R.B.; investigation: S.E. (Safae Elmisaoui) and L.K.; writing—original draft preparation: S.E. (Safae Elmisaoui), L.K., R.B. and S.B.; writing—review and editing, S.E. (Safae Elmisaoui) and R.B.; visualization, S.E. (Safae Elmisaoui), R.B. and S.E. (Sanae Elmisaoui); supervision, L.K., M.K. and S.B.; project administration: L.K. and S.B.; funding acquisition: L.K. and S.B. All authors have read and agreed to the published version of the manuscript.

Institutional Review Board Statement: Not applicable.

Informed Consent Statement: Not applicable.

References

1. Dittmar, H. Fertilizers, 4. Granulation. In *Ullmann's Encyclopedia of Industrial Chemistry*; Wiley-VCH: Weinheim, Germany, 2000.
2. Artyukhov, A.; Sklabinskyi, V. Hydrodynamics of gas flow in small-sized vortex granulators in the production of Nitrogen fertilizers. *Chem. Chem. Technol.* **2015**, *9*, 337–342. [CrossRef]
3. Saleh, K.; Guigon, P. Mise en œuvre des Poudres: Techniques de Granulation Humide et Liants. Techniques de l'ingénieur. Génie des Procédés, J2253. 2009. Available online: https://www.techniques-ingenieur.fr/base-documentaire/biomedical-pharma-th15/mise-en-forme-des-medicaments-et-autres-produits-de-sante-42611210/mise-en-uvre-des-poudres-j2254/ (accessed on 13 June 2022).
4. Ntamo, D.; Lopez-Montero, E.; Mack, J.; Omar, C.; Highett, M.I.; Moss, D.; Mitchell, N.; Soulatintork, P.; Moghadam, P.Z.; Zandi, M. Industry 4.0 in Action: Digitalisation of a Continuous Process Manufacturing for Formulated Products. *Digit. Chem. Eng.* **2022**, *3*, 100025. [CrossRef]
5. Le, V.G.; Vo, D.V.N.; Nguyen, N.H.; Shih, Y.J.; Vu, C.T.; Liao, C.H.; Huang, Y.H. Struvite recovery from swine wastewater using fluidized-bed homogeneous granulation process. *J. Environ. Chem. Eng.* **2021**, *9*, 105019. [CrossRef]
6. Liu, B.; Wang, J.; Zeng, J.; Zhao, L.; Wang, Y.; Feng, Y.; Du, R. A review of high shear wet granulation for better process understanding, control and product development. *Powder Technol.* **2021**, *381*, 204–223. [CrossRef]
7. Elmisaoui, S.; Khamar, L.; Benjelloun, S.; Khamar, M.; Ghidaglia, J.M. Numerical Study of fertilizer granules dynamics within rotary drum granulator. In *Computer Aided Chemical Engineering*; Elsevier: Amsterdam, The Netherlands, 2021; Volume 50, pp. 327–332.
8. Vesjolaja, L.; Glemmestad, B.; Lie, B. Application of population balance equation for continuous granulation process in spherodizers and rotary drums. In Proceedings of the SIMS 2020 Virtual, Finland , 22–24 September 2021.
9. Elmisaoui, S.; Elmisaoui, S.; Benjelloun, S.; Khamar, L.; Khamar, M. CFD Investigation of Industrial Gas-liquid Preneutralizer Based on a Bioreactor Benchmark for Spargers Optimization. *Chem. Eng. Trans.* **2022**, *93*, 73–78.
10. Elmisaoui, S.; Khamar, L.; Benjelloun, S.; Khamar, M.; Ghidaglia, J. Modeling and Study of Hydrodynamic flow within the Preneutralizer Reactor using CFD Approach. In *Computer Aided Chemical Engineering, Proceedings of the 30th European Symposium on Computer Aided Process Engineering, Milan, Italy, 24–27 May 2020*; Elsevier:Amsterdam, The Netherlands, 2020; Volume 48, pp. 103–108.
11. Fertahi, S.; Ilsouk, M.; Zeroual, Y.; Oukarroum, A.; Barakat, A. Recent trends in organic coating based on biopolymers and biomass for controlled and slow release fertilizers. *J. Control. Release* **2021**, *330*, 341–361. [CrossRef] [PubMed]
12. Yang, R.Y.; Yu, A.B.; McElroy, L.; Bao, J. Numerical simulation of particle dynamics in different flow regimes in a rotating drum. *Powder Technol.* **2008**, *188*, 170–177. [CrossRef]
13. Govender, I. Granular flows in rotating drums: A rheological perspective. *Miner. Eng.* **2016**, *92*, 168–175. [CrossRef]
14. Arntz, M.M.H.D.; den Otter, W.K.; Briels, W.J.; Bussmann, P.J.T.; Beeftink, H.H.; Boom, R.M. Granular mixing and segregation in a horizontal rotating drum: A simulation study on the impact of rotational speed and fill level. *AIChE J.* **2008**, *54*, 3133–3146. [CrossRef]
15. Pathmathas, T. Granular Flow Modelling of Rotating Drum Flows Using Positron Emission Particle Tracking. Ph.D. Thesis, University of Cape Town, Cape Town, South Africa, 2015.
16. Santos, D.A.; Scatena, R.; Duarte, C.R.; Barrozo, M.A.S. Transition phenomenon investigation between different flow regimes in a rotary drum. *Braz. J. Chem. Eng.* **2016**, *33*, 491–501. [CrossRef]
17. Nascimento, S.M.; Lima, R.M.; Brandão, R.J.; Duarte, C.R.; Barrozo, M.A.S. Eulerian study of flights discharge in a rotating drum. *Can. J. Chem. Eng.* **2019**, *97*, 477–484. [CrossRef]
18. Santos, D.A.; Barrozo, M.A.S.; Duarte, C.R.; Weigler, F.; Mellmann, J. Investigation of particle dynamics in a rotary drum by means of experiments and numerical simulations using DEM. *Adv. Powder Technol.* **2016**, *27*, 692–703. [CrossRef]
19. Kasper, J.H.; Magnanimo, V.; de Jong, S.D.M.; Beek, A.; Jarray, A. Effect of viscosity on the avalanche dynamics and flow transition of wet granular matter. *Particuology* **2021**, *59*, 64–75. [CrossRef]
20. Burgos-Florez, F.; Bula, A.; Marquez, J.; Ferrer, A.; Sanjuan, M. CFD-DEM modeling and simulation coupled to a global thermodynamic analysis methodology for evaluating energy performance: Biofertilizer industry. *Processes* **2019**, *7*, 673. [CrossRef]
21. Baba, T.; Nakamura, H.; Takimoto, H.; Ohsaki, S.; Watano, S.; Takehara, K.; Higuchi, T.; Hirosawa, T.; Yamamoto, T. DEM–PBM coupling method for the layering granulation of Iron ore. *Powder Technol.* **2021**, *378*, 40–50. [CrossRef]
22. Zhao, J.; Shan, T. Numerical modeling of fluid-particle interaction in granular media. *Theor. Appl. Mech. Lett.* **2013**, *3*, 021007. [CrossRef]

23. Hayashi, K.; Nakamura, H.; Watano, S. Numerical study on granule aggregation and breakage in fluidized bed granulation by a novel PBM with DEM-CFD coupling approach. *Powder Technol.* **2020**, *360*, 1321–1336. [CrossRef]

24. Delele, M.A.; Weigler, F.; Franke, G.; Mellmann, J. Studying the solids and fluid flow behavior in rotary drums based on a multiphase CFD model. *Powder Technol.* **2016**, *292*, 260–271. [CrossRef]

25. Nieuwland, J.J.; van Sint Annaland, M.; Kuipers, J.A.M.; van Swaaij, W.P.M. Hydrodynamic modeling of gas/particle flows in riser reactors. *AIChE J.* **1996**, *42*, 1569–1582. [CrossRef]

26. Wang, W.; Lu, B.; Geng, J.; Li, F. Mesoscale drag modeling: A critical review. *Curr. Opin. Chem. Eng.* **2020**, *29*, 96–103. [CrossRef]

27. Du, W.; Bao, X.; Xu, J.; Wei, W. Computational fluid dynamics (CFD) modeling of spouted bed: Assessment of drag coefficient correlations. *Chem. Eng. Sci.* **2006**, *61*, 1401–1420. [CrossRef]

28. Upadhyay, M.; Kim, A.; Kim, H.; Lim, D.; Lim, H. An Assessment of Drag Models in Eulerian–Eulerian CFD Simulation of Gas–Solid Flow Hydrodynamics in Circulating Fluidized Bed Riser. *ChemEngineering* **2020**, *4*, 37. [CrossRef]

29. Schiller, L.; Naumann, A. A drag coefficient correlation. *Z. Vereins Dtsch. Ingenieure* **1935**, *77*, 318–320.

30. Helland, E.; Bournot, H.; Occelli, R.; Tadrist, L. Drag reduction and cluster formation in a circulating fluidised bed. *Chem. Eng. Sci.* **2007**, *62*, 148–158. [CrossRef]

31. Wen, C.Y.; Yu, H.Y. Chemical engineering progress symposium series. *Mech Fluid* **1966**, *62*, 100–111.

32. Gidaspow, D. *Multiphase Flow and Fluidization: Continuum and Kinetic Theory Descriptions*; Academic Press: Cambridge, MA, USA, 1994.

33. Syamlal, M.; O'Brien, T.J. *The Derivation of a Drag Coefficient Formula from Velocity-Voidage Correlations*; Technical Note; US Department of energy, Office of Fossil Energy, NETL: Morgantown, WV, USA, 1987.

34. Khalilitehrani, M.; Abrahamsson, P.J.; Rasmuson, A. Modeling dilute and dense granular flows in a high shear granulator. *Powder Technol.* **2014**, *263*, 45–49. [CrossRef]

35. Chao, Z.; Wang, Y.; Jakobsen, J.P.; Fernandino, M.; Jakobsen, H.A. Investigation of the particle–particle drag in a dense binary fluidized bed. *Powder Technol.* **2012**, *224*, 311–322. [CrossRef]

36. Lun, C.K.K. Kinetic theory for granular flow of dense, slightly inelastic, slightly rough spheres. *J. Fluid Mech.* **1991**, *233*, 539–559. [CrossRef]

37. Schaeffer, D.G. Instability in the evolution equations describing incompressible granular flow. *J. Differ. Equ.* **1987**, *66*, 19–50. [CrossRef]

38. Chmielewski, M.; Gieras, M. Three-zonal wall function for k-ε turbulence models. *Comput. Methods Sci. Technol.* **2013**, *19*, 107–114. [CrossRef]

39. Hou, Z.; Zhao, Y. Numerical and experimental study of radial segregation of bi-disperse particles in a quasi-two-dimensional horizontal rotating drum. *Particuology* **2020**, *51*, 109–119. [CrossRef]

40. Santos, D.A.; Petri, I.J.; Duarte, C.R.; Barrozo, M.A.S. Study of hybrid drag models for predicting hydrodynamic behaviour in a spouted bed. *Can. J. Chem. Eng.* **2013**, *11*, 1776–1785. [CrossRef]

41. Adnan, M.; Sun, J.; Ahmad, N.; Wei, J.J. Validation and sensitivity analysis of an Eulerian–Eulerian two-fluid model (TFM) for 3D simulations of a tapered fluidized bed. *Powder Technol.* **2022**, *396*, 490–518. [CrossRef]

42. Santos, D.A.; Petri, I.J.; Duarte, C.R.; Barrozo, M.A.S. Experimental and CFD study of the hydrodynamic behavior in a rotating drum. *Powder Technol.* **2013**, *250*, 52–62. [CrossRef]

43. Tamburini, A.; Cipollina, A.; Micale, G.; Brucato, A.; Ciofalo, M. Influence of drag and turbulence modelling on CFD predictions of solid liquid suspensions in stirred vessels. *Chem. Eng. Res. Des.* **2014**, *92*, 1045–1063. [CrossRef]

44. Alagha, M.S.; Szentannai, P. Experimentally-assessed multi-phase CFD modeling of segregating gas–solid fluidized beds. *Chem. Eng. Res. Des.* **2021**, *172*, 215–225. [CrossRef]

45. Wu, X.; Zuo, Z.; Gong, S.; Lu, X.; Xie, G. Numerical study of size-driven segregation of binary particles in a rotary drum with lower filling level. *Adv. Powder Technol.* **2021**, *32*, 4765–4778. [CrossRef]

46. Rahman, R.; Zhu, H.; Yu, A. Numerical analysis of effects of specularity coefficient and restitution coefficient on the Hydrodynamics of particles in a rotating Drum. *Processes* **2022**, *10*, 167. [CrossRef]

47. Sandadi, S.; Pandey, P.; Turton, R. In situ, near real-time acquisition of particle motion in rotating pan coating equipment using imaging techniques. *Chem. Eng. Sci.* **2004**, *59*, 5807–5817. [CrossRef]

48. Norouzi, H.R.; Zarghami, R.; Mostoufi, N. Insights into the granular flow in rotating drums. *Chem. Eng. Res. Des.* **2015**, *102*, 12–25. [CrossRef]

49. Li, S.Q.; Yan, J.H.; Li, R.D.; Chi, Y.; Cen, K.F. Axial transport and residence time of MSW in rotary kilns: Part I. Experimental. *Powder Technol.* **2002**, *126*, 217–227. [CrossRef]

50. Rogers, R.S.C.; Gardner, R.P. A Monte Carlo method for simulating dispersion and transport through horizontal rotating cylinders. *Powder Technol.* **1979**, *23*, 159–167. [CrossRef]